

Adsorption of Silver from Aqueous Solution with High Capacity and Selectively by Using Ag⁺ Imprinted Polymeric Nanoadsorbent

Veyis Karakoç,[✉]*^a Cem Esen[✉]^b and Adil Denizli[✉]^c

^aVocational School of Health Services, Çankırı Karatekin University, 18200, Çankırı, Turkey

^bDepartment of Chemistry, Aydın Adnan Menderes University, 09010, Aydın, Turkey

^cDepartment of Chemistry, Hacettepe University, 06800, Ankara, Turkey

The selective separation of precious metals from complex aqueous solutions is important in protecting the environment, aquatic ecosystems, water resources and recycling resources. In this study, cysteine-containing polymeric nanoparticles were synthesized using the molecular imprinting (MIP) technique with the mini-emulsion polymerization method. The basis of the polymer design is inspired by affinity of silver to cysteine in biological systems. The synthesized silver ion imprinted (Ag⁺-IIP) poly(hydroxyethylmethacrylate-*N*-methacryloyl-L-cysteine) poly(HEMA-MAC) nanoparticles were characterized by elemental analysis, zeta sizer, Fourier transform infrared (FTIR) spectroscopy, atomic force microscopy (AFM), and scanning electron microscopy (SEM). The effects of pH, ionic strength and interaction time on adsorption of Ag⁺ ions were investigated. In experimental studies, the highest adsorption amount (196.9 mg g⁻¹ nanoparticle) was reached in a short period of 40 min at pH 5.0 and 150 mg L⁻¹ concentration. Selectivity studies of synthesized Ag⁺-IIP nanoparticles against silver (Ag⁺) ions were carried out in the presence of lithium (Li⁺), barium (Ba²⁺), mercury (Hg²⁺) and cadmium (Cd²⁺) ions. Experimental results indicate that nanoparticles adsorb Ag⁺ ions with high selectivity. Ag⁺-IIP nanoparticles have 3.7, 3.1, 2.4, and 2.6 times more selective or higher affinity for Ag⁺ ions compared to Li⁺, Ba²⁺, Hg²⁺ and Cd²⁺ ions, respectively, compared to Ag⁺-non-imprinted (NIP) nanoparticles.

Keywords: Ag⁺ silver adsorption, nanoparticles, affinity adsorption, ion-imprinted polymer

Introduction

Silver, a precious element, dates back to 3100 Before Christ (BC) in ancient Egypt and has been used as an ornament or coin throughout history. Silver is often used because of its antibacterial effect and is a good conductor of heat and electricity. Due to these properties, silver is widely used in many fields such as photography, medical imaging (X-ray, etc.), electrical industry, dentistry, porcelain production, production of medical instruments, ink production and ornaments production.¹⁻³ Because of its widespread use in industry, silver has been included in the food chain through wastewater. Acute or chronic ingestion of silver at high concentrations threatens human health (argyria and argyrosis) and aquatic ecosystems. The World Health Organization (WHO) has determined the maximum

concentration of silver in waters to be 100 ppm and stated that values above it harm health.⁴⁻⁶

It is essential to recover silver due to its economic value and toxic environmental effects. Electrochemical precipitation, ion exchange, ultra-filtration, adsorption and reverse osmosis methods are used to recover silver from wastewater. The adsorption method comes into prominence due to the shortcomings of other methods such as high cost, low selectivity, time-consuming and high labour.^{7,8} The adsorption method has attracted attention in recent years and has become an area on which researchers work intensively because the adsorbent can be reused and especially the shapes and surface properties of polymeric adsorbents can be adjusted as desired.

The most critical criteria for adsorbents prepared for the removal of heavy metals from wastewater are the capacity of the adsorbent, the selective adsorption, and its short duration. These criteria can be achieved more efficiently, especially with nanoparticles.⁹⁻¹¹ The fact that nanoparticles have very high surface areas compared to their masses has

*e-mail: veyiskarakoc@karatekin.edu.tr

Editor handled this article: Fernando C. Giacomelli (Associate)



allowed access to high adsorption capacities in adsorption processes. Especially in the enrichment and separation processes of precious metals, nanoparticles come to the fore as a good adsorbent. The fact that the surface properties of polymeric nanoparticles allow for modification also enables them to be used as selective adsorption agents. In recent years, polymeric nanoparticles prepared using the molecular imprinting technique have been used in many areas such as adsorption, catalysis, sensors, drug carriers, etc.¹²⁻¹⁵

Molecular imprinting is a technique to create recognition sites in synthetic materials by mimicking recognition processes in biological systems. Recognition processes in biological systems occur using non-covalent, weak secondary interactions. Hydrogen bonding, hydrophobic interaction, electrostatic interactions, Van der Waals interactions, and metal chelate coordination interactions are also used in the recognition processes of polymeric materials prepared using this method.^{16,17}

While preparing ion-imprinted polymers for metal recognition, interactions of metals with monomers with electron-donating sulfur, nitrogen or oxygen (S, N or O) atoms are considered. In the application process of the ion imprinting method, monomer selection is made according to the target ion, taking into account the Soft Acid-Base Theory defined by Pearson.¹⁸ Polymeric adsorbents prepared by molecular imprinting method have many advantages compared to highly selective immuno-adsorbents, such as low cost, workability under harsh conditions, reusability, long shelf life and preparation in desired form (film, sphere, bulk, etc.).¹⁹⁻²²

In the present study, inspired by the knowledge that silver ions interact with thiol groups in the human body and accumulate in tissues, a biologically based functional monomer *N*-methacryloyl-L-cysteine (MAC) was prepared. The affinity of silver to sulfhydryl (-SH) groups was considered based on the adsorption strategy. The selectivity of nanoparticles to silver ions was increased by using the ion imprinting method. In this study, polymeric nanoparticles with -SH functional groups for rapid and high-capacity adsorption of Ag⁺ ions were synthesized in nanosize. The usability of the synthesized nanoparticles in the selective separation and recovery of high amounts of silver ions in the presence of other metal ions was investigated.

Experimental

Materials

For the synthesis of MAC monomer, methacryloyl chloride and L-cysteine was supplied from Sigma (St. Louis, USA) and used as received. The monomers

hydroxyethyl methacrylate (HEMA) and ethylene glycol dimethacrylate (EGDMA) were obtained from Sigma Chem. Co. (St. Louis, USA) and stored at 4 °C until use. Sodium dodecyl sulphate (SDS), sodium bicarbonate (NaHCO₃), sodium bisulfite (NaHSO₃) ammonium persulfate (APS, 98%) and poly(vinyl alcohol) PVA (98% hydrolyzed, molecular weight 100.000 Da) were purchased from Sigma Chem. Co. (St. Louis, Missouri, USA) and used as the surfactant and steric stabilizer of the polymerization. Silver nitrate (AgNO₃) salt was used as ion template source (Merck Co., Darmstadt, Germany). The remaining chemicals were reagent grades purchased from Merck AG (Darmstadt, Germany). All water used in the experiments was purified using a Barnstead ROpure LP[®] reverse osmosis unit (Dubuque, IA, USA) with a high-flow cellulose acetate membrane (Barnstead D2731) followed by a Barnstead D3804 NANOpure[®] organic/colloid removal and ion exchange packed bed system. The purified water (deionized water) has a specific conductivity of 18 MΩ cm.

Synthesis of MAC monomer and MAC-Ag complex

The synthesis of MAC monomer was adapted from the procedure reported in the literature.²³ According to the relevant procedure, 5.0 g of L-cysteine and 0.2 g of sodium nitrite (NaNO₂) (Sigma Chem. Co. St. Louis, Missouri, USA) were dissolved in 30 mL of potassium carbonate (K₂CO₃) aqueous solution (5%, v/v) (Sigma Chem. Co. St. Louis, Missouri, USA), and the mixture was cooled to 0 °C. Four millilitres of methacryloyl chloride was poured dropwise into this solution while stirring slowly under a nitrogen atmosphere, and then the reaction was performed at room temperature for 2 h. After the reaction, the solution's pH was adjusted to 7.0, and then methacryloyl chloride was extracted with ethyl acetate. The aqueous phase was evaporated in a rotary evaporator. The residue (MAC) was dissolved in ethanol. Figure 1 shows the synthesis of MAC monomer from L-cysteine amino acid.

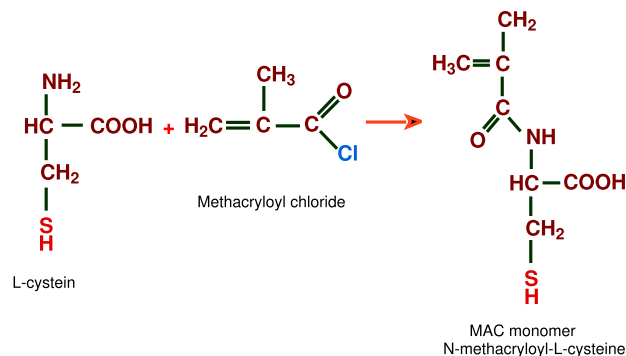


Figure 1. Schematic illustration of the synthesis of MAC monomer from L-cysteine amino acid.

Two moles of MAC solution in ethanol were treated with one mole of Ag⁺ solution at room temperature for 2 h to provide a monomer-template complex as MAC-Ag⁺.

Synthesis and characterization studies of nanospheres

In order to synthesize molecularly imprinted polymers (MIP), the MAC-Ag complex was first formed at 2 mmol/1 mmol rates.²⁴ Silver nitrate (AgNO₃) salt was used to form the MAC-Ag complex. Figure 2 shows the predicted interaction with MAC monomers and Ag⁺ ions in the formation of the MAC-Ag complex.

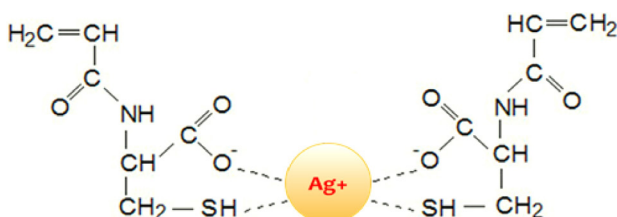


Figure 2. Predicted interaction with MAC monomers and Ag⁺ ions in the formation of the MAC-Ag complex.

Poly(HEMA-MAC) nanoparticles were synthesized using the mini-emulsion method using methacrylamidocysteine (MAC) and 2-hydroxyethyl methacrylate (HEMA). Firstly, 0.375 g of PVA, 57.7 mg of SDS and 46.9 mg of NaHCO₃ were dissolved in 20 mL of deionized water to form the first aqueous phase. The second aqueous phase was prepared as a dispersion medium by dissolving 0.2 g of PVA and 0.2 g of SDS in 400 mL of water. Then, 0.2 mg of Ag-MAC complex was mixed to form 0.9 mL of HEMA and 4.2 mL of crosslinker EGDMA organic phase. Then, the mixture was stirred with a magnetic stirrer at 200 rpm for 15 min to form a mini-emulsion. This mixture was poured to the second aqueous phase of 400 mL. The final mixture was transferred to a 500 mL three-necked glass flask and heated to 50 °C at 500 rpm by stirring. By adding 0.230 g of NaHSO₃ and 0.252 g of APS to the reaction medium, polymerization was carried out for 24 h. Figure 3 shows a schematic representation of the mini-emulsion polymerization system used to prepare silver ion imprinted (Ag⁺-IIP) nanoparticles. After the cooling process of the reactor, the synthesized nanoparticles were removed from the medium by centrifuging at 30,000 rpm and precipitating. Unreacted monomers and surfactants such as SDS and PVA were entirely removed by washing with an ethanol-water (70% v/v) mixture. Ag⁺-non-imprinted nanoparticles (NIP) were also synthesized using the same method without template ions. The synthesized polymers were lyophilized, dried after washing, and stored in room conditions.

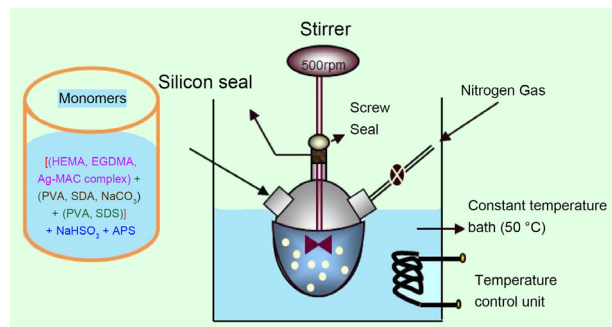


Figure 3. Schematic representation of the mini-emulsion polymerization system used in the preparation of Ag⁺-IIP nanoparticles.

Fourier transform infrared (FTIR) analysis (FTIR 8000 Series, Shimadzu, Shimadzu Corp. Kyoto, Japan) was performed to identify the composition of the chemical functional groups of the polymer. The synthesized nanoparticles were characterized both in size and shape using a scanning electron microscope (SEM). Topographic images of the surfaces of nanoparticles were obtained using a scanning electron microscope (SEM, Carl Zeiss Microscopy GmbH 73447 Oberkochen, Germany) and an atomic force microscope (AFM, Nanomagnetics Instruments, Oxford, UK). The sizes of the synthesized nanoparticles were analyzed with Nano Zetasizer (NanoS, Malvern Instruments, London, UK). 1 mL of suspended Ag⁺-IIP nanoparticles was placed in the cell of the zeta size measuring device for measuring, and the results were evaluated after the analysis.

The MAC content of synthesized polymeric Ag⁺-IIP nanoparticles was determined using Flash 2000 CHNS/O Elemental Analyzer (Thermo Fisher Scientific Inc., Waltham, MA, USA).

Surface area calculation

The equation giving the number of particles in 1 mL suspension was used to calculate the surface area of the synthesized Ag⁺-IIP nanoparticles (equation 1).

$$N = 6 \times 10^{10} \times S/\pi \times \rho_s \times d^3 \quad (1)$$

where N is the number of nanoparticles in 1 mL suspension; S (%) is solids; d diameter (nm); and ρ_s indicates the polymer density (g mL⁻¹). The specific surface area of Ag⁺-IIP nanoparticles synthesized using the surface area equation was calculated in m² g⁻¹.

Adsorption of Ag⁺ ions from aqueous solution

Adsorption of Ag⁺ ions from aqueous solutions was studied in batch mode using Ag⁺-IIP nanoparticles. Before the experimental studies, 250 mL stock solutions were

prepared at 500 mg L⁻¹ concentrations containing Ag⁺ ions. The stock solutions were diluted in 10-fold dilutions to the concentration determined for experimental studies (5 mg L⁻¹).

The synthesized Ag⁺-IIP nanoparticles were frozen in suspension and dried in a lyophilization device (Christ Freeze Dryer-Alpha 1-2 LD, Maryland, USA). The dried nanoparticles were weighed, and their amounts were determined. Then, they were sonicated by ultrasonic water bath (Bransonic 2200, England) in 25 mL of deionized water, redispersed, and suspended. Thus, homogeneous nanoparticle solutions were prepared, and the mass amounts of nanoparticles used in experimental studies were determined. The amounts of Ag⁺ ions adsorbed *per* unit mass of the nanoparticles (mg metal ions *per* g nanoparticles) were evaluated using equation 2.

$$\text{Ag}^+ \text{ adsorbed} = (C_i - C_f)V/m1000 \quad (2)$$

where, C_i and C_f are the concentrations of the Ag⁺ ions in the aqueous medium before and after the adsorption period, respectively (mg L⁻¹); V is the volume of the aqueous adsorption medium (mL); and m is the amount of the polymer used (g).

The effects of initial silver concentration on adsorption, medium pH, temperature and adsorption time were investigated. The effect of initial silver concentration on adsorption was investigated by changing the silver concentration between 0.5-250 mg L⁻¹, and the effect of pH on adsorption was changed between pH 2.0 and 8.0. Concentrations of silver ions in aqueous solutions were determined using ICP-OES (inductively coupled plasma optical emission spectrometry) (Teledyne Leemans Labs Prism model, Hudson, NH, USA) (ICP-OES Teledyne Leeman Labs Prism Model axial vision ICP-OES). The parameters of the device used in the analysis of metal ions are given in Table 1. Experiments were repeated at least three times. The confidence interval was taken as 95%. Standard statistical methods were applied to calculate each data set's mean values and standard deviation.

Selectivity studies

Competitive adsorption experiments were carried out in an aqueous solution to demonstrate the selectivity of Ag⁺-IIP nanoparticles. Lithium (Li⁺), barium (Ba²⁺), mercury (Hg²⁺) and cadmium (Cd²⁺) ions were chosen as competitor ions. The Li⁺, Ba²⁺, Hg²⁺ and Cd²⁺ ions were selected as the competitor ions because they have the same ionic charge and nearly identical ionic radius and bind well with the -SH groups. Ag⁺ ions were added to the competing ion mixtures. The selectivity experiments

Table 1. The operating conditions of ICP-OES instrument were used to analyze silver ions

Parameter	
Nebulizer	concentric glass
Spray chamber	cyclonic
R.F. power / kW	1.1
Auxiliary gas (Ar) flow rate / (L min ⁻¹)	0.5
Coolant gas (Ar) flow rate / (L min ⁻¹)	19.0
Nebulizer flow / psi	34
Sample uptake rate / (mL min ⁻¹)	1.4
Wavelength / nm	232.468

were conducted for Ag⁺-IIP nanoparticles with solutions containing 100 mg L⁻¹ concentration of ion mixture (total volume: 100 mL) at a stirring speed of 250 rpm for 2 h.

The distribution coefficients (K_d) for Li⁺, Ba²⁺, Hg²⁺ and Cd²⁺ concerning Ag⁺ were calculated by equation 3.

$$K_d = ((C_i - C_f)C_p)V/m \quad (3)$$

where K_d represents the distribution coefficient for the metal ion (mL g⁻¹), C_i and C_f are the initial and final concentrations of the metal ion (mg L⁻¹), respectively, V is the volume of the solution (mL), m is the weight of the polymeric nanoparticles used for adsorption (g).

The selectivity coefficient (k) for the binding of Ag⁺ in the presence of the competing species (Li⁺, Ba²⁺, Hg²⁺ and Cd²⁺) was determined by equation 4.

$$k = K_{d(\text{template metal ion})}/K_{d(\text{competing metal ion})} \quad (4)$$

where K_{d(template metal ion)} is the distribution coefficient of the template ion (Ag⁺), and K_{d(competing metal ion)} is the distribution coefficient of the competing metal ions (Li⁺, Ba²⁺, Hg²⁺ and Cd²⁺).

A ratio of the selectivity coefficients (k') in equation 5, in which k_{imprinted} is for the Ag⁺-IIP (HEMA-MAC) in the presence of the Ag⁺/Li⁺, Ag⁺/Ba²⁺, Ag⁺/Hg²⁺ and Ag⁺/Cd²⁺ ion pairs and k_{non-imprinted} is for the Ag⁺non-IIP poly(HEMA-MAC) in the presence of the Ag⁺/Li⁺, Ag⁺/Ba²⁺, Ag⁺/Hg²⁺ and Ag⁺/Cd²⁺ ion pairs, is the relative selectivity coefficient, which was used to estimate the effect of imprinting on the ion selectivity.

$$k' = k_{\text{imprinted}}/k_{\text{non-imprinted}} \quad (5)$$

Desorption and repeated use

Desorption of Ag⁺ ions was carried out with desorption agents: 0.1 M nitric acid (HNO₃) (pH 4.0) (Merck Co., Darmstadt, Germany) solution containing 0.05% thiourea

solution (Sigma Chem. Co. St. Louis, Missouri, USA). The Ag⁺-IIP poly(HEMA-MAC) nanoparticles were placed in this desorption medium and stirred continuously (at a stirring rate of 400 rpm) for 2 h at room temperature to desorb silver ions. The desorption ratio was calculated from the amount of Ag⁺ ions adsorbed by the nanoparticles and the final Ag⁺ ion concentration in the desorption medium. The reusability of Ag⁺-IIP nanoparticles was determined by applying the adsorption-desorption procedure repeated 10 times on the same particles. The nanoparticles were washed with 0.1 M sodium hydroxide (NaOH) (Sigma Chem. Co. St. Louis, Missouri, USA) solution to regenerate the nano adsorbent.

Results and Discussion

Characterization studies

Structure analysis with FTIR

Figure 4 shows the FTIR spectra of the MAC monomer, Ag-IIP poly(HEMA-MAC) nanoparticles. In the FTIR spectrum of Ag-IIP nanoparticles, hydrogen O–H stretching peak is observed at 3367 cm⁻¹, carbonyl band at 1710 cm⁻¹, aliphatic C–H band at 2951 cm⁻¹, amide I and amide II bands at 1635 and 1447 cm⁻¹ respectively. In addition, the specific S–H stretching vibration is observed at 930 and 890 cm⁻¹.^{20,25,26}

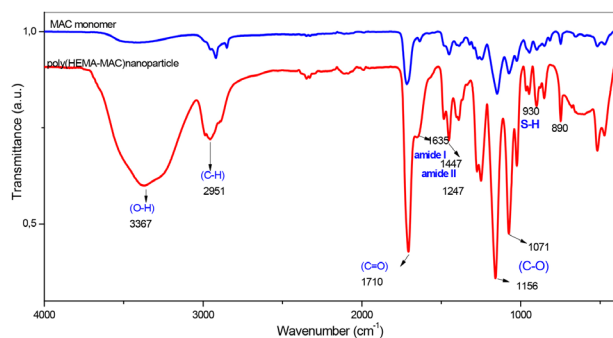


Figure 4. FTIR-ATR spectra of MAC monomer, Ag⁺-IIP poly (HEMA MAC) nanoparticles.

Particle size analysis

Figure 5 shows a screenshot of size analysis instruments belonging to synthesized Ag⁺-IIP nanoparticles. It was observed from the zeta size analysis of the synthesized nanoparticles that the mean diameter was 98.9 nm and had an equivalent size range. The size analysis of the synthesized Ag⁺-IIP nanoparticles was conducted by preparing the suspension solutions after the nanoparticles were synthesized and washed.

Polydispersity index (PDI) measurement was performed to determine the size distribution of the synthesized

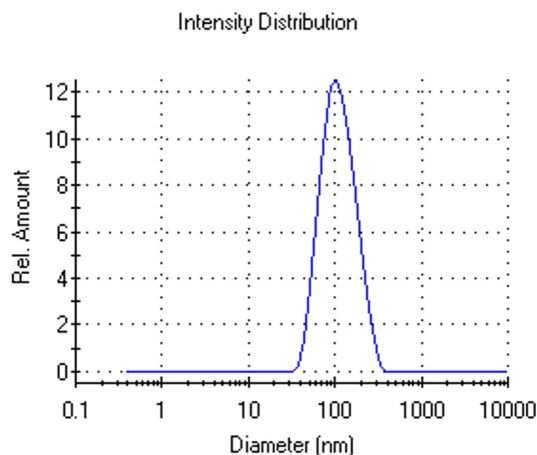


Figure 5. Size analysis of synthesized Ag⁺-IIP nanoparticles.

nanoparticles. When the PDI value, which measures the size distribution range and heterogeneity of the particles, is less than 0.05, the particles are expressed as monodisperse size distribution. The polydispersity value of the synthesized nanoparticles was measured as PDI 0.156. Since this value is far from the heterogeneous distribution value > 0.7 and is close to the monodispersity value, it indicates that the synthesized nanoparticles are almost equidimensional and monodisperse. It can also be said that the synthesized nanoparticles are composed of molecules with the same mass.

The PDI value of the synthesized nanoparticles also gives us information about the width of the molecular weight distribution (MWD). From the PDI value obtained, it can be stated that the synthesized nanoparticle particles consist of homologous monomer sequences with the same molecular weights.

Surface analysis with SEM

The surface morphology of Ag⁺-IIP nanoparticles was investigated by scanning electron microscopy. Ag⁺-IIP nanoparticles were used in SEM analysis. From SEM photographs of dry Ag⁺-IIP nanoparticles, the nanoparticles are almost monosize, smooth, and spherical (Figure 6). It was determined from the SEM images that the dimensions of the nanoparticles were around 80 nm.

Surface analysis with AFM

AFM images of the synthesized nanoparticles were obtained by scanning the nanoparticles *per* unit area (2 μm × 2 μm). Ag⁺-IIP nanoparticles were used in AFM analysis. Figure 7 shows an AFM photograph of Ag⁺-IIP nanoparticles. Although small aggregations occur due to the use of centrifuges in washing the synthesized nanoparticles, it has been observed that the nanoparticles are monosize, smooth, and spherical, with a maximum size of 86.2 nm.

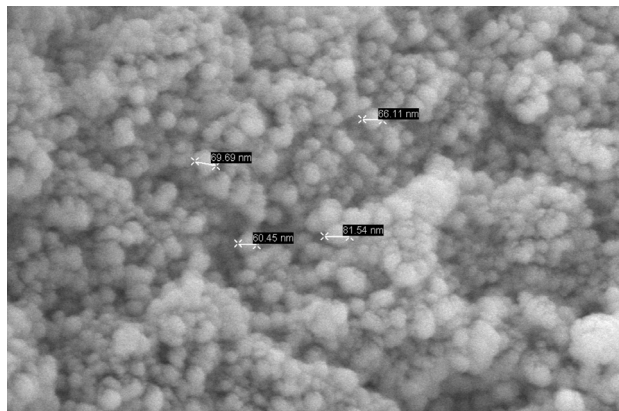


Figure 6. SEM photograph of Ag⁺-IIP nanoparticles.

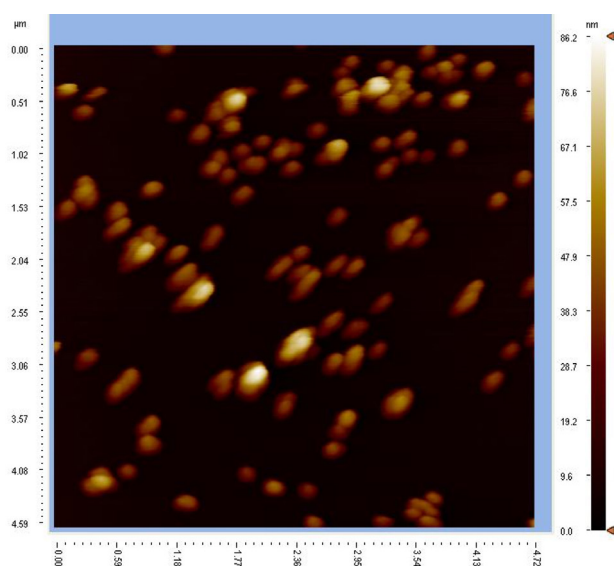


Figure 7. AFM photograph of Ag⁺-IIP nanoparticles.

Calculation of surface areas of nanoparticles

The specific surface areas of the synthesized Ag⁺ imprinted nanoparticles were calculated using equation 1 and found to be 872 m² g⁻¹ dry nanoparticles. These high surface areas of nanoparticles quickly allow for high adsorption capacities in adsorption processes in a very short time.

Elemental analysis of nanoparticles

Using the data obtained from the elemental analysis study, stoichiometric calculations were made, and the MAC content of polymeric nanoparticles was calculated as 7.3 mmol MAC g⁻¹ polymer. It should be noted here that the monomer HEMA and the crosslinker EGDMA do not contain nitrogen or sulfur atoms. The (S) atom and (N) atom sources seen in elemental analysis of the polymer only incorporate MAC monomers.

Adsorption studies of silver ions

Effect of pH on adsorption

Figure 8 shows the adsorption of Ag⁺ ion to Ag⁺-IIP nanoparticles at different pH values. pH is an essential parameter in removing metal ions from water by adsorption. Depending on the pH of the medium, the charge of the adsorbent and the analyte also changes. As previously stated, the -SH groups of the MAC monomer in the structure of polymeric nanoparticles interact with Ag⁺ ions. The isoelectric point of the cysteine amino acid in the polymer is pI: 4.9. In other words, the polymeric structure is negatively charged at pHs above pI and positively charged at pHs below. As seen in Figure 8, the maximum adsorption occurs at a pH close to the natural water pH (pH: 5.0-6.0).

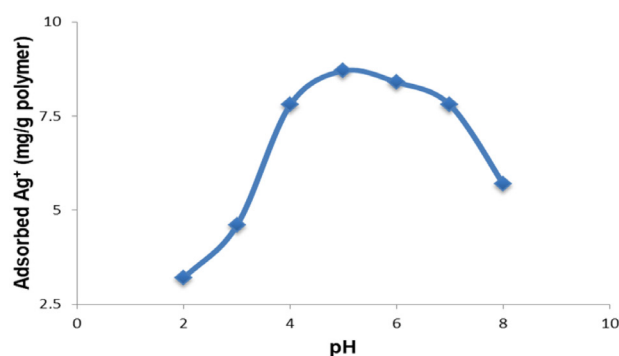


Figure 8. Effect of pH on Ag⁺ adsorption. Volume: 25 mL, initial concentration: 5 mg L⁻¹; time: 2 h, temperature: 25 °C.

Effect of initial concentration on adsorption

It is easier for target ions (Ag⁺) to bind to the ion-recognizing regions on the surfaces of adsorbents prepared by ion imprinting. In the experimental study, silver solutions with 0.5-300 mg L⁻¹ concentrations were used to determine the adsorption capacity of Ag⁺-IIP nanoparticles. As seen in Figure 9, with the increase of the silver initial concentration in the solution, the amount

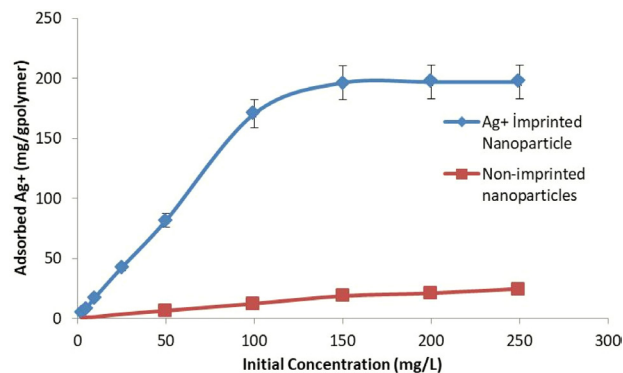


Figure 9. Effect of Ag⁺ initial concentration on Ag⁺ adsorption. Volume: 25 mL, pH: 5.0, time: 2 h, temperature: 25 °C.

of silver adsorbed *per unit* Ag⁺-IIP nanoparticle increased rapidly. It reached equilibrium at an initial concentration of approximately 150 mg L⁻¹. The concentration difference (ΔC), the driving force for adsorption, increases with increasing concentration. It was observed that the adsorption capacity increased depending on the increase in the driving force. The maximum adsorption capacity of Ag⁺-IIP nanoparticles for an initial silver concentration of 150 mg L⁻¹ is 196.9 mg Ag⁺ g⁻¹ dry nanoparticle. The adsorption rate of Ag⁺IIP nanoparticle was recorded as 97% for 50 mg L⁻¹ silver solution.

Effect of interaction time on adsorption

Figure 10 shows the adsorption of Ag⁺ ions depending on time. One of the most important advantages of nano-sized materials is the rapid adsorption due to their high surface area. Ag⁺ ions in the medium were adsorbed on the surface in the first 40 min. It can be seen from Figure 10 that, unlike conventional adsorbents, the maximum adsorption is reached in a very short time since the diffusion of the target ion into the pores in the adsorbent does not occur in nanoparticles. As expected, the adsorption capacity reached equilibrium in the first 40 min due to filling the formed cavities where the analyte can bind on the adsorbent surface obtained by the Ag⁺ ion imprinting method. During this period, the maximum adsorption amount for Ag⁺ ions is 9.48 mg g⁻¹ dry IIP nanoparticles.

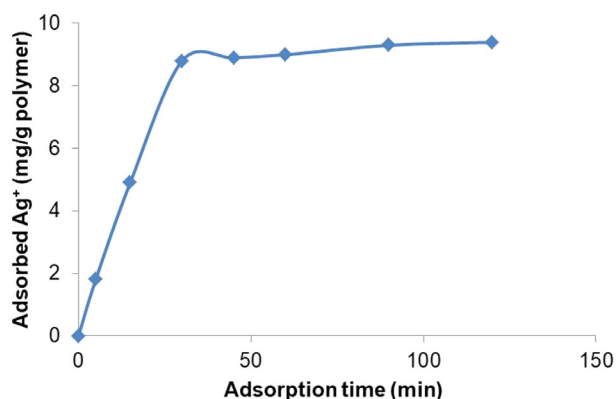


Figure 10. Time-dependent change of Ag⁺ adsorption on Ag⁺-IIP nanoparticles. Volume: 25 mL, initial concentration: 5 mg L⁻¹; pH: 5.0, temperature 25 °C.

Selectivity experiments

To determine the selectivity of Ag⁺-IIP and NIP nanoparticles, competitive adsorption experiments were carried out in an aqueous solution. In the study, ions (Li⁺, Ba²⁺, Hg²⁺, Cd²⁺) close to Ag⁺ ion in terms of charge and ion diameter were selected. A polymeric nano adsorbent

was prepared using the molecular imprinting technique to increase the selectivity of the adsorbent to the silver ion. Initial concentrations of ions in the adsorption medium were prepared as 100 mg L⁻¹.

Selectivity and relative selectivity coefficients (*k* and *k'* values) were calculated for Ag⁺-IIP and Ag⁺-NIP nanoparticles. As a result of the analysis, it was calculated that the *k* values of Ag⁺-IIP nanoparticles were higher than the *k* values of the non-imprinted nanoparticle in the presence of competitive ions. The relative selectivity coefficient *k'* is an indicator for expressing the adsorption affinity of Ag⁺ ions to the recognition cavities created by the molecular imprinting technique on the adsorbent surface.

According to the *k'* results in Table 2, Ag⁺-IIP nanoparticles have 3.7, 3.1, 2.4 and 2.6 times more selective or higher affinity for Ag⁺ ions compared to Li⁺, Ba²⁺, Hg²⁺ and Cd²⁺ ions, respectively, than NIP nanoparticles. As seen in Figure 11, Ag⁺-IIP nanoparticles adsorbed Ag⁺ ions in higher amounts than Li⁺, Ba²⁺, Hg²⁺ and Cd²⁺ ions. NIP nanoparticles also exhibit a similar adsorption tendency. It can be concluded that the Ag⁺-IIP nanoparticles show the following metal ion affinity order under competitive adsorption conditions: Ag⁺ > Hg²⁺ > Cd²⁺ > Ba²⁺ > Li⁺.

Table 2. Calculated selectivity coefficients, distribution coefficient and relative selectivity values of competitive ions with respect to silver ions

Competitive ion	Polymer				
	Ag ⁺ -IIP nanoparticles		Ag ⁺ -non-IIP nanoparticles		
	Kd	k	Kd	k	k'
Ag ⁺	128.2		16.3		
Li ⁺	11.8	10.8	5.5	2.9	3.7
Ba ²⁺	24.3	5.3	9.4	1.7	3.1
Hg ²⁺	43.7	2.9	13.2	1.2	2.4
Cd ²⁺	38.1	3.3	11.7	1.4	2.6

Kd: distribution coefficient; *k*: selectivity coefficient; *k'*: relative selectivity coefficient (A ratio of the selectivity coefficients).

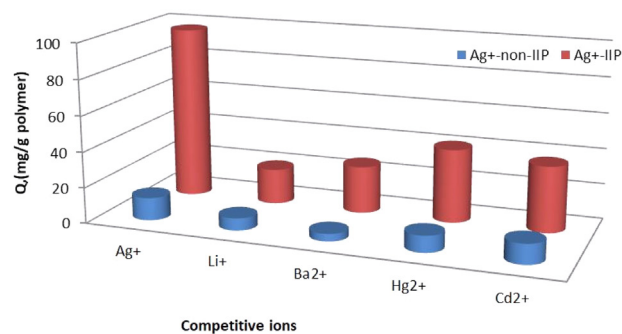


Figure 11. Selectivity studies of Ag⁺-IIP nanoparticles in the presence of competitive ions.

Adsorption of Ag⁺ ions from real sample

Waste radiographic films were obtained from the X-ray unit of the orthopedic clinic of a local hospital. The waste radioactive films were cut into small pieces (2 cm × 2 cm). The film pieces were washed with water and ethyl alcohol and then dried at room temperature. 2 g of the washed X-ray films were weighed and added to 100 mL of 1 M HNO₃ solution. The film's nitric acid solution was mixed in the fume hood using a mechanical stirrer at 80 °C for 2 h. The films were removed from the solution when the colors of the films became transparent. After the solution was cooled, it was diluted 1/10 using deionized water. The Ag⁺ concentration in the initial solution was determined by taking an initial sample. Then, 30 mL of silver solution was taken into the beaker, and Ag⁺-IIP nanoparticles were added, and the mixture was mixed in a magnetic stirrer for 3 h. The nanoparticle solution was centrifuged at the end of the adsorption process, and the nanoparticles were precipitated. Finally, the amount of Ag⁺ in the final sample was determined by measuring it with ICP-OES. The calculations showed that 96.7% of the Ag⁺ ions in the solution environment were adsorbed by the nanoparticles using Ag⁺-IIP nanoparticles.

Desorption and reusability

Reusability studies were carried out in 5 mg L⁻¹ Ag⁺ ion solution. It was desorbed from the polymer using an Ag⁺ desorption agent, which was adsorbed on nanoparticles. 97% desorption of adsorbed silver was achieved. For the desorption of Ag⁺ ions from nanoparticles, 0.01 M HNO₃ (pH 4.0) solution containing 0.05% thiourea was used as the desorption agent. To determine the reusability of Ag⁺-IIP nanoparticles, the adsorption-desorption process was repeated at least 10 times using the same nanoparticle. The adsorption-desorption cycle showing the reusability of Ag⁺-IIP nanoparticles is given in Figure 12.

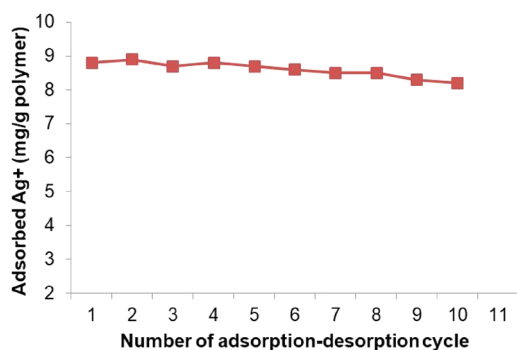


Figure 12. Reusability of Ag⁺-IIP nanoparticles.

Literature comparison

Studies on the removal and recovery of silver from wastewater in the literature were mainly carried out using the adsorption method. For this purpose, adsorbents with very different properties, such as polymeric or inorganic microbeads, magnetic particles, membranes or spongy cryogels, have been developed. In addition, studies to develop adsorbents of biological origin have gained importance. The primary strategy in developing adsorbents with different properties is to consider the basic properties of the adsorbent, such as working in harsh conditions, having high adsorption capacity, being economical and reusable, and being selective. It has been observed that high adsorption capacity can be achieved thanks to the high surface area of the nanoparticles. The most common strategy used for selective adsorption is the use of the molecular imprinting technique as well as surface modification of the adsorbent. In the literature, while preparing adsorbents for the selective adsorption of silver ions, adsorbents with –SH groups on the surface were synthesized due to the affinity of silver for sulfur. Table 3 summarizes the adsorption capacities of the adsorbents based on adsorption and generally prepared by the imprinting method, from the studies conducted on silver ions in the literature.

Conclusions

Silver is an element that has always been used throughout human history. Today, due to its widespread usage, it has also entered the food chain. In addition, it also pollutes drinking and environmental waters and has become a threat to living organisms. In addition to the economic value of silver, it is also essential to separate and remove it from wastewater because it has a toxic effect on biological systems. In the literature, the accumulation of silver as a complex due to its affinity for cysteine in biological systems is a subject that has been extensively researched and clarified.

In current studies inspired by biological systems, nanoparticles with –SH functional groups on the surface were synthesized. The presence of a –SH-containing monomer (MAC) in the synthesized polymeric backbone provides significant advantages to the adsorbent. The use of MAC monomer while preparing the polymer eliminates deficiencies like ligand leakage that occurs in adsorbents where functional groups are added to the surface later. This approach also eliminates the need for extra processing steps, such as activation and the immobilization of functional groups onto the surface of the adsorbents.

Table 3. Comparison of the silver adsorption efficacy of different adsorbents in the literature

Material/adsorbent	Max. adorp. Q	Reference
Ag ⁺ imprinted magnetic thiourea-chitosan nanoparticles	4.93 mmol g ⁻¹	7
O-Phenanthroline-based granül polymer	325.8 mg g ⁻¹	8
Aza-thioether crown containing Ag ⁺ -IIP (Phen S ₂ N(CH ₃), L) nanoparticle	18.08 mmol g ⁻¹	27
Surface-activated carbon nanospheres	152 mg g ⁻¹	28
Ion-imprinted polymer-modified silica-coated magnetite nanoparticles	28.2 mg g ⁻¹	29
Sulfoethyl functionalized silica nanoparticle	21.9 mg g ⁻¹	30
Nitrogen and sulfur-decorated carbon dots	714.3 mg g ⁻¹	31
Halloysite nanotubes	109.79 mg g ⁻¹	32
Ag ⁺ ion-imprinting (Ag-IISHPs) hollow particles	80.5 mg g ⁻¹	33
Low-rank Turkish coals	1.87 mg g ⁻¹	34
Thiol-rich, porous activated carbon (AC)	719.2 mg g ⁻¹	35
Almond shell-activated carbon (ASC)	59.52 mg g ⁻¹	36
Ag ⁺ -imprinted chitosan based biosorbent	199.2 mg g ⁻¹	37
Magnetic ion-imprinted (Fe ₃ O ₄ @SiO ₂ @TiO ₂ -IIP) polymeric nanoparticles	35.475 mg g ⁻¹	38
Ion imprinted 1-VID-EBA _m / 4-VP-EBA _m polymeric particles	75.64 mg g ⁻¹ / 74.18 mg g ⁻¹	39
Ag ⁺ ions imprinted polymeric cryogels	49.27 mg g ⁻¹	40
Ion-imprinting chitosan/poly(vinyl alcohol) PVA membrane	125 mg g ⁻¹	41
Thiourea groups bearing polyvinylidene fluoride (PVDF) membrane	1.6 mmol g ⁻¹	42
Allylthiothionine functionalized (3-AR/PVDF) micro-filtration membrane	46.42 mg (cm ²) ⁻¹	43
Sulfur or nitrogen containing microalgal gels	2.40/2.70 mmol g ⁻¹	44
Ag-imprinted chitosan/triethanolamine (CTS/TEA) composites hydrogel (Ag-ICTHB) (Ag-ICTGB) bead	510 / 350 mg g ⁻¹	45
Amine/thio functionalized magnetic chelating resin	6,2 mmol g ⁻¹	46
Dithiooxamide-formaldehyde (DFOB) resin	3333.3 mg g ⁻¹	47
Melamine-formaldehyde-thiourea (MFT) chelating resin	60.05 mg g ⁻¹	48
Ag ⁺ -imprinted poly(HEMA-MAC) polymeric nanoparticles	196.9 mg g ⁻¹	this study

Molecular imprinting technology, a technique to increase the selectivity properties of adsorbents, was used in the selective removal of silver ions from water. In this way, the affinity and selectivity of the synthesized nanoparticles to silver ions were increased. Thanks to the nanoparticles prepared using the molecular imprinting technique, the rapid adsorption of silver ions with a very high capacity was selectively carried out according to similar studies in the literature. In addition, synthesizing adsorbents in nano sizes significantly contributed to the adsorption capacity and shortening of the adsorption time. The results suggest that Ag IIP nanoparticles can be an effective nano adsorbent for removing silver from aqueous solution due to their high selectivity, adsorption capacity, and short processing time. In addition to all these, the fact that the adsorbent can be regenerated and used again and again without significant decreases in its adsorption ability makes it economical. It is expected that this study will provide a new perspective to the researchers in this field as well as making significant contributions to the literature.

Author Contributions

In this study, V. K. and C. E. were responsible for experiments, concept, design, investigation, syntheses, characterization, methodology, software, validation, analytical measurements, writing-original draft preparation, analysis and interpretation of results of the article; and A. D. have contributed to analysis and interpretation of results writing-review, editing, preparation of the draft and final draft. All authors reviewed the results and approved the final version of the manuscript.

References

1. Eckelman, M. J.; Graedel, T. E.; *Environ. Sci. Technol.* **2007**, *41*, 6283. [Crossref]
2. Garcia-Reyero, N.; Kennedy, A. J.; Escalon, B. L.; Habib, T.; Laird, J. G.; Rawat, A.; Wiseman, S.; Hecker, M.; Denslow, N.; Steevens, J. A.; Perkins, E. J.; *Environ. Sci. Technol.* **2014**, *48*, 4546. [Crossref]
3. Ratte, H. T.; *Environ. Toxicol. Chem.* **1999**, *18*, 89. [Crossref]

4. Gnanadhas, D. P.; Thomas, M. B.; Thomas, R.; Raichur, A. M.; Chakravorty, D.; *Antimicrob. Agents Chemother.* **2013**, *10*, 4945. [Crossref]
5. Antsiferova, A. A.; Kashkarov, P. K.; Koval'chuk, M. V.; *Nanotechnol. Russ.* **2022**, *17*, 155. [Crossref]
6. Lansdown, A. B. G.; *Adv. Pharmacol. Pharm. Sci.* **2010**, ID 910686. [Crossref]
7. Fan, L.; Luo, C.; Lv, Z.; Lu, F.; Qiu, H.; *J. Hazard. Mater.* **2011**, *194*, 193. [Crossref]
8. Ding, X.; Yu, W.; Sheng, X.; Shi, H.; You, D.; Peng, M.; Shao, P.; Yang, L.; Liu, L.; Luo, X.; *Chin. Chem. Lett.* **2023**, *34*, 107485. [Crossref]
9. Khan, I.; Saeed, K.; Khan, I.; *Arabian J. Chem.* **2019**, *12*, 908. [Crossref]
10. Uygun, M.; Feyzioglu, E.; Ozcaliskan, E.; Caka, M.; Ergen, A.; Akgol, S.; Denizli, A.; *J. Nanopart. Res.* **2013**, *15*, 1833. [Crossref]
11. Karakoc, V.; *Hacettepe J. Biol. Chem.* **2020**, *48*, 319. [Crossref]
12. Erdem, Ö.; Saylan, Y.; Andaç, M.; Denizli, A.; *Biomimetics* **2018**, *3*, 38. [Crossref]
13. Say, R.; Erdem, M.; Ersöz, A.; Türk, H.; Denizli, A.; *Appl. Catal., A* **2005**, *286*, 221. [Crossref]
14. Sarı, E.; Üzek, R.; Duman, M.; Denizli, A.; *Talanta* **2016**, *150*, 607. [Crossref]
15. Yıldırım, M.; Acet, Ö.; Yetkin, D.; Acet, B.Ö.; Karakoc, V.; Odabasi, M.; *J. Drug Delivery Sci. Technol.* **2022**, *74*, 103552. [Crossref]
16. Uzun, L.; Turner, A. P. F.; *Biosens. Bioelectron.* **2016**, *76*, 131. [Crossref]
17. BelBruno, J. J.; *Chem. Rev.* **2019**, *119*, 94. [Crossref]
18. Pearson, R. G.; *J. Am. Chem. Soc.* **1963**, *85*, 3533 [Crossref]
19. Rajabi, H. R.; Zarezadeh, A.; Karimipour, G.; *RSC Adv.* **2017**, *7*, 14923. [Crossref]
20. Rezaei, M.; Rajabi, H. R.; Rafiee, Z.; *Colloids Surf., A* **2020**, *586*, 124253. [Crossref]
21. Shamsipur, M.; Rajabi, H. R.; *Microchim. Acta* **2013**, *180*, 243. [Crossref]
22. Rajabi, H. R.; Shamsipur, M.; Pourmortazavi, S. M.; *Mater. Sci. Eng., C* **2013**, *33*, 3374. [Crossref]
23. Denizli, A.; Say, R.; Garipcan, B.; Emir, S.; Karabakan, A.; Patir, S.; *Sep. Purif. Technol.* **2003**, *30*, 3. [Crossref]
24. Leung, B. O.; Jalilehvand, F.; Mah, V.; Parvez, M.; Wu, Q.; *Inorg. Chem.* **2013**, *52*, 4593. [Crossref]
25. Sheydaei, O.; Khajehsharifi, H.; Rajabi, H. R.; *Sens. Actuators, B* **2020**, *309*, 127559. [Crossref]
26. Zarezadeh, A.; Rajabi, H. R.; Sheydaei, O.; Khajehsharifi, H.; *Mater. Sci. Eng., C* **2019**, *94*, 879. [Crossref]
27. Shamsipur, M.; Hashemi, B.; Dehdashtian, S.; Mohammadi, M.; Gholivand, M. B.; Garau, A.; Lippolis, V.; *Anal. Chim. Acta* **2014**, *852*, 223. [Crossref]
28. Song, X.; Gunawan, P.; Jiang, R.; Leong Su, J. S.; Wang, K.; Xu, R.; *J. Hazard. Mater.* **2011**, *194*, 162. [Crossref]
29. Kazemi, E.; Mohammad, A.; Shabani, H.; Dadfarnia, S.; *Microchim. Acta* **2015**, *182*, 1025. [Crossref]
30. Zhang, L.; Zhang, G.; Wang, S.; Peng, J.; Cui, W.; *J. Taiwan Inst. Chem. Eng.* **2017**, *71*, 330. [Crossref]
31. Asiabi, H.; Yamini, Y.; Shamsayei, M.; Molaie, K.; Shamsipur, M.; *J. Hazard. Mater.* **2018**, *357*, 217. [Crossref]
32. Kiani, G.; *Appl. Clay Sci.* **2014**, *90*, 159. [Crossref]
33. Hou, H.; Yu, D.; Hu, G.; *Langmuir* **2015**, *31*, 1376. [Crossref]
34. Karabakan, A.; Karabulut, S.; Denizli, A.; Yurum, Y.; *Adsorpt. Sci. Technol.* **2004**, *22*, 135. [Crossref]
35. Yao, Z.; Shao, P.; Fang, D.; Shao, J.; Li, D.; Liu, L.; Huang, Y.; Yu, Z.; Yang, L.; Yu, K.; Luo, X.; *J. Chem. Eng.* **2022**, *427*, 131470. [Crossref]
36. Omri, A.; Benzina, M.; *Desalin. Water Treat.* **2013**, *51*, 2317. [Crossref]
37. Huo, H.; Su, H.; Tan, T.; *Chem. Eng. J.* **2009**, *150*, 139. [Crossref]
38. Yin, X.; Long, J.; Xi, Y.; Luo, X.; *ACS Sustainable Chem. Eng.* **2017**, *5*, 2090. [Crossref]
39. Ahamed, MEH.; Mbianda, X. Y.; Mulaba-Bafubiandi, A. F.; Marjanovic, L.; *React. Funct. Polym.* **2013**, *73*, 474. [Crossref]
40. Şarkaya, K.; Bakhshpour, M.; Denizli, A.; *Sep. Sci. Technol.* **2018**, *54*, 2993. [Crossref]
41. Shawky, H. A.; *J. Appl. Polym. Sci.* **2009**, *114*, 2615. [Crossref]
42. Liu, P.; Wang, X.; Tian, L.; He, B.; Lv, X.; Li, X.; Wang, C.; Song, L.; *J. Water Process Eng.* **2020**, *34*, 101184. [Crossref]
43. Yin, X.; Zhang, Q.; Yang, L.; Geng, Z.; Luo, X.; Ren, W.; *Chem. Eng. J.* **2022**, *443*, 136376. [Crossref]
44. Khunathai, K.; Inoue, K.; Ohto, K.; Kawakita, H.; Kurata, M.; Atsumi, K.; Fukuda, H.; Alam, S.; *Materials* **2017**, *10*, 636. [Crossref]
45. Zhang, L.; Yang, S.; Han, T.; Zhong, L.; Ma, C.; Zhou, Y.; Han, X.; *Appl. Surf. Sci.* **2012**, *263*, 696. [Crossref]
46. Atia, A. A.; Donia, A. M.; Heniesh, A. M.; *Sep. Sci. Technol.* **2014**, *49*, 2039. [Crossref]
47. Çelik, Z.; Gülfen, M.; Aydın, A. O.; *J. Hazard. Mater.* **2010**, *174*, 556. [Crossref]
48. Yirikoglu, H.; Gülfen, M.; *Sep. Sci. Technol.* **2008**, *43*, 376. [Crossref]

Submitted: February 11, 2024

Published online: June 10, 2024